

# Iron-based superconductivity extended to the novel hydride LaFeSiH

F. Bernardini,<sup>1</sup> G. Garbarino,<sup>2</sup> A. Sulpice,<sup>3</sup> M. Núñez-Regueiro,<sup>3</sup>  
E. Gaudin,<sup>4</sup> B. Chevalier,<sup>4</sup> A. Cano,<sup>4,\*</sup> and S. Tencé<sup>4</sup>

<sup>1</sup>*CNR-IOM-Cagliari and Dipartimento di Fisica,  
Università di Cagliari, IT-09042 Monserrato, Italy*

<sup>2</sup>*European Synchrotron Radiation Facility, 6 rue Jules Horowitz, BP 220, 38043 Grenoble, France*

<sup>3</sup>*CNRS, Université Grenoble Alpes, Institut Néel, 38042 Grenoble, France*

<sup>4</sup>*CNRS, Univ. Bordeaux, ICMCB, UPR 9048, F-33600 Pessac, France*

(Dated: December 13, 2024)

We report the synthesis and characterization of the novel hydride LaFeSiH displaying superconductivity below 8.5 K. We find that this pnictogen-free compound is isostructural to LaFeAsO, with a similar low-temperature tetragonal to orthorhombic distortion. Using density functional theory we show that this system is also a multiband metal in which the orthorhombic distortion is likely related to single-stripe antiferromagnetic order. Electrical resistivity and magnetic susceptibility measurements reveal that these features occur side-by-side with superconductivity, which is suppressed by external pressure.

Iron-based superconductors (Fe-based SCs) provide an unprecedented playground for the investigation of high- $T_c$  superconductivity. These systems belong to a huge family of compounds and recurrently display the following key features (see e.g. [1] for recent reviews). From the structural point of view, they have FeX layers in which the Fe atoms form a square lattice that is sandwiched between two ( $\sqrt{2} \times \sqrt{2}$ ) $R45^\circ$  shifted lattices of  $X$  ( $=$  P, As, Se, Te, S). This leads to a quasi-2D multiband Fermi surface that mainly originates from the Fe 3d orbitals. In addition, the parent compounds often display anti-ferromagnetic (AFM) order which is closely followed by a structural transformation (the so-called nematic transition). In the prototypical case of  $R\text{FeAsO}$  ( $R$  = rare earth), for example, this specifically corresponds to single-stripe AFM order [also called  $(\pi, 0)$  order] and a square-to-rectangular distortion of the Fe layers. These features advocate for the so-called  $s_\pm$  superconducting gap symmetry and a spin-fluctuation pairing. This superconductivity can be induced by carrier doping resulting from either chemical substitutions or physical pressure [2]. From a more methodological point of view, the electronic band structure and the magnetic orders found in Fe-based SC can be reasonably well described by means of DFT-based calculations as the electronic correlations often remain relatively weak.

The search for novel Fe-based SC has been naturally extended to systems in which the FeX layer contains group IV elements such as Si and Ge. Thus, MgFeGe for example has been identified as isostructural and iso-electronic to the LiFeAs compound but displaying no superconductivity [3–5]. Furthermore, among the different substitutions inducing superconductivity, hydrogen substitution has proven to be particularly interesting. Specifically, the carrier doping limit of the original F substitution in LaFeAsO has been surpassed with hydrogen, which reveals a two-dome superconductivity [6] and eventually a second magnetic phase in the additional parent

compound LaFeAsO<sub>0.5</sub>H<sub>0.5</sub> [7]. In this paper, we report the synthesis, crystal structure and physical properties of the novel compound LaFeSiH. In addition, we study the behavior of the system under hydrostatic pressure and perform density-functional-theory (DFT) calculations to obtain the corresponding electronic band structure and magnetic ground state of this compound. Thus, we find that the new compound LaFeSiH is isostructural, iso-electronic and also “isomagnetic” to the 1111 family of Fe-based SC. Most importantly, we find superconductivity below 8.5 K in this pnictide- and chalcogenide-free system.

*Crystal structure.*— We synthesized the hydride LaFeSiH as described in the Supplemental Material. The compound is stable in air, and its room-temperature crystal structure corresponds to the tetragonal space group  $P4/nmm$  with the structural parameters shown in Table I. This structure was determined from the Rietveld refinement of the x-ray powder diffraction pattern and more accurately from single-crystal x-ray diffraction measurements (see Fig. 1 and Supplemental Material). Compared to LaFeSi [8], the new compound displays a variation of the lattice parameters that is highly anisotropic:  $a = 4.098 \rightarrow 4.027$  Å and  $c = 7.133 \rightarrow 8.014$  Å. This variation is due to the hydrogen insertion at the  $2b$  Wyckoff position, as observed in other CeFeSi-type hydrogenated intermetallics [9]. This insertion is confirmed from the single-crystal x-ray diffraction pattern. Additionally, we performed DFT calculations in which we confirmed that the  $2b$  position is a very stable position for the H atom. Specifically, the overall  $P4/nmm$  structure is found to have a well-defined phonon spectrum with H-related optical phonons of frequencies greater than 100.5 meV. Thus, we conclude that the room-temperature crystal structure of LaFeSiH is essentially the same structure of the 1111 Fe-based SCs (e.g. LaFeAsO) as illustrated in Fig. 1.

We also determined the low-temperature crystal structure by performing additional x-ray synchrotron exper-

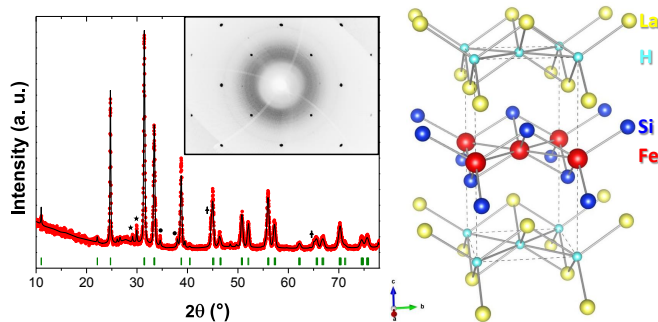


FIG. 1. (Left) Room temperature X-ray powder diffraction pattern of LaFeSiH. Ticks indicate the Bragg peaks of the  $P4/nmm$  structure of the main LaFeSiH phase while stars, crosses and circles indicate extra peaks due to the secondary phases  $\text{La}_2\text{O}_3$ ,  $\alpha\text{-Fe}$  and  $\text{La}(\text{Fe},\text{Si})_{13}\text{H}_x$  respectively that could not be completely eliminated by annealing. The  $(hk0)$ -plane of the LaFeSiH single-crystal diffraction pattern at room temperature is shown in the inset. (Right) Ball-and-stick model of the crystal structure of LaFeSiH.

iments at 15 K. The refinement of the corresponding structure revealed a low-temperature phase of LaFeSiH with space group symmetry  $Cmma$ . The structural parameters of this phase are in Table I. The orthorhombic distortion is rather small, which is again similar to the observed in Fe-based SCs.

*Electronic and magnetic structure.*— We first computed the electronic structure of LaFeSiH assuming a non-magnetic ground state (see Supplemental Material for details). We took the experimental low-temperature structural parameters as input. However, since the orthorhombic distortion is very small, we averaged the  $a$  and  $b$  parameters and considered an effective tetragonal structure. In Fig. 2 (top-right) we show the calculated electronic density of states (DOS) and the partial DOS (PDOS) projected on the Fe  $3d$  orbitals. As we can see, the system has a metallic nature with a DOS at the Fermi level that is largely dominated by the Fe- $3d$  orbitals. The corresponding band structure is shown in Fig. 2 (top-left), where the size of the symbols reflects the PDOS of the  $3(d_{xz} + d_{yz})$  Fe orbitals. This structure reveals the presence of several bands crossing the Fermi energy, which renders the system a multiband character. Specifically, we have two hole bands centered at the  $\Gamma$  point and two additional bands around the  $M$  point. In addition, there is a third band centered at the  $\Gamma$  point below the Fermi energy but very close. The resulting Fermi surface is shown in Fig. 2 (bottom). This Fermi surface has a resemblance to the characteristic Fermi surface of the Fe-based SCs. The central lobe originating from the outer hole band and the belly of the otherwise cylindrical electron sheets represent the main differences.

The nesting properties of the LaFeSiH Fermi surface are limited compared to most of Fe-based SCs. Yet this system can develop some type of magnetic order. Thus,

293K - $P4/nmm$ (#129, origin 2)				
$a = 4.0270(1)\text{\AA}$ $c = 8.0374(8)\text{\AA}$				
	Wyckoff pos.	$x$	$y$	$z$
La	$2c$	1/4	1/4	0.6722(1)
Fe	$2a$	3/4	1/4	0
Si	$2c$	1/4	1/4	0.1500(5)
H	$2b$	3/4	1/4	1/2

15K - $Cmma$ (#67)				
$a = 5.6831(6)\text{\AA}$ $b = 5.7039(6)\text{\AA}$ $c = 7.9728(6)\text{\AA}$				
	Wyckoff pos.	$x$	$y$	$z$
La	$4g$	0	1/4	0.1747(3)
Fe	$4b$	1/4	0	0
Si	$4g$	0	1/4	0.655(1)
H	$4a$	1/4	0	0

TABLE I. Structure parameters of LaFeSiH. (293K) Positions obtained from single-crystal x-ray diffraction with cell parameters obtained from measurements on powder samples. The single-crystal diffraction pattern reveals the  $2b$  position of the H atom. Its refinement, however, is restricted to the La, Fe, and Si atoms. (15K) Parameters obtained from Rietvel refinements of x-ray synchrotron data.

we performed additional DFT calculations in which different magnetic states were considered. Specifically, we study the tendency of the non-magnetic tetragonal structure towards ferromagnetic (FM), single-stripe AFM, double-stripe AFM and checkerboard AFM ordering of the Fe spins. The energy difference with respect to the non-magnetic state and the corresponding magnetic mo-

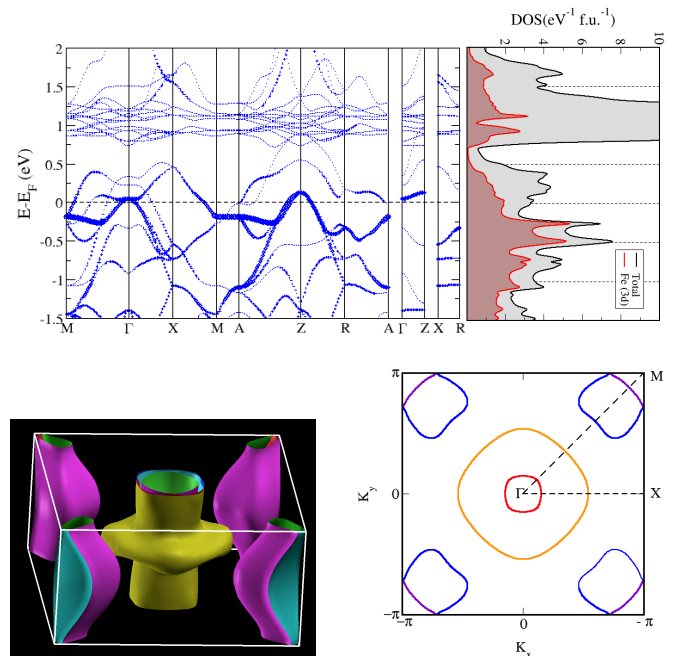


FIG. 2. (Top-left) Band structure and (top-right) total DOS and PDOS of the Fe- $3d$  states. (Bottom-left) Three dimensional view of the Fermi surface and (bottom-right) cross section in the  $k_z = 0$  plane.

ments are reported in Table II. We find that the single-stripe AFM order reduces considerably the total energy of the system, and therefore is expected to be the ground state of the system. This explains the orthorhombic distortion we observed experimentally, as this is expected to be a by-product of the single-stripe AFM order triggered by magnetostructural coupling [10, 11].

*Crystal and magnetic structure under pressure.*— Next, we study the orthorhombic low-temperature structure of the system under external pressure. In Fig. 3 we show the evolution of the orthorhombic distortion at 15 K obtained from our x-ray synchrotron measurements. We find that this distortion is suppressed by the application of external pressure and eventually disappears at  $P_{c1} \simeq 9.4$  GPa. This is similar to the observed in most of Fe-based SCs. Interestingly, by further increasing the pressure the structural distortion re-emerges at  $P_{c2} \simeq 12.7$  GPa. This behavior strongly resembles the observed in LaFeAsO by means of H doping [7].

In order to elucidate the nature of the high-pressure state we performed additional DFT calculations as a function of pressure for the aforementioned magnetic configurations. In these calculations, the single-stripe AFM state was always found to be the lowest-energy state. In Fig. 4 we show the resulting Fe magnetic moment and the energy difference with respect to the non-magnetic state as a function of pressure. Although the precise numerical values depend on the DFT method, they are in remarkably good agreement with the experimental observations. Namely, the application of external pressure first produces the suppression of single-stripe AFM order which then re-emerges as the pressure is further increased. Moreover, according to these results, the re-emergence is expected to be discontinuous. The reason is that, even if a non-vanishing Fe magnetic moment is developed, the energy of the single-stripe AFM state requires some extra pressure to eventually become lower than the energy of the non-magnetic state. The structural distortion observed in our experiments, however, displays rather continuous behavior. Note that this distor-

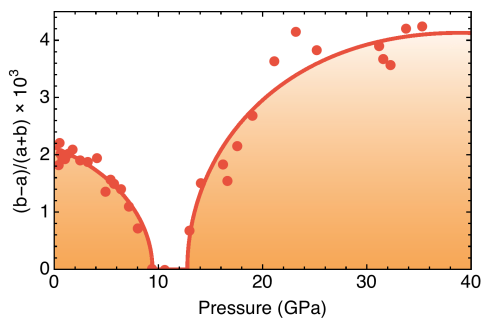


FIG. 3. Relative difference between the  $a$  and  $b$  lattice parameters of LaFeSiH at 15K as a function of pressure. Lines are guides to the eye.

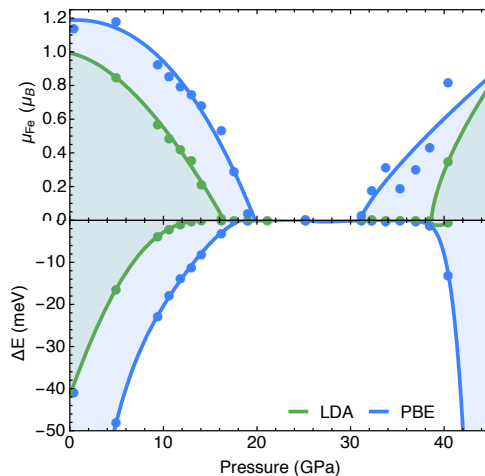


FIG. 4. Calculated Fe magnetic moment in the single-stripe AFM state (top) and energy difference with respect to the non-magnetic state (bottom) as a function of pressure. The results obtained with LDA and PBE functionals are represented by blue and green points respectively. Lines are guides to the eye.

tion is just a by-product of the magnetic order induced by magnetostructural coupling, and hence is quite small. Consequently, the magnetic discontinuity expected from the DFT calculations could be very difficult to observe indirectly via the lattice distortion. In any case, these calculations are remarkably consistent with the structural behavior observed in our x-ray experiments (see Fig. 3).

*Magnetization and electrical resistivity.*— Last, in the search for superconductivity, we performed magnetization and electrical resistivity measurements. The magnetic response of LaFeSiH clearly reveals the emergence of superconductivity in this compound. Specifically, the magnetization as a function of the magnetic field at 2 K has a very strong negative slope of  $dM/dH \sim -2.5 \times 10^{-3}$  uem/g [see Fig. 5 (a)]. This slope changes at  $\sim 4$  Oe, which indicates a critical field  $H_{c1} \sim 2.5$  Oe. The smallness of this field is likely due to defects and/or the presence of secondary magnetic phases like  $\text{La}(\text{Fe},\text{Si})_{13}\text{H}_x$  responsible for the zero-field initial magnetization at low temperature. Furthermore, the temperature dependence of the magnetization at 10 Oe is in tune with a typical superconducting behavior with a transition temperature  $T_c = 8.5$  K [Fig. 5 (b)]. Indeed, the positive offset due to the initial magnetization is over-compensated at low temperatures in the ZFC measurement. The corresponding

	checkerboard	FM	double-stripe	single-stripe
$\Delta E$ (meV/Fe)	-5.71	-11.11	-11.26	-44.56
$\mu_{\text{Fe}}$ ( $\mu_{\text{B}}$ )	0.90	0.65	1.04	1.16

TABLE II. Energy difference with respect to the non-magnetic state and Fe magnetic moments for various magnetic configurations obtained from DFT calculations.

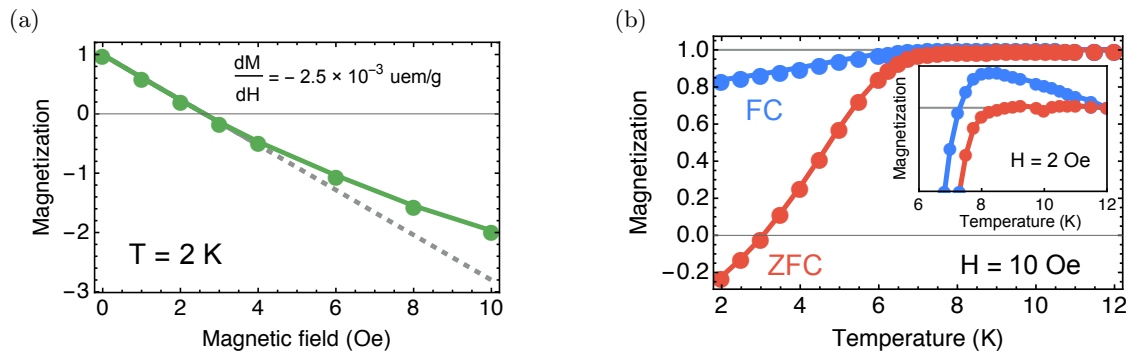


FIG. 5. (a) Magnetization as a function of the external field at 2 K normalized to its zero-field value. The very high negative susceptibility  $dM/dH = -2.5 \times 10^{-3}$  uem/g confirms the emergence of superconductivity. (b) Magnetization as a function of temperature at  $H = 10$  Oe normalized to the value 0.057 uem/g measured at 12 K. The inset shows the temperature behavior at  $H = 2$  Oe. The clear diamagnetic behavior observed in these curves reveals the onset of superconductivity at 8.5 K.

change in the magnetization between the normal state at 9 K and the superconducting state at 2 K is  $\sim 0.017$  uem/g at 2 Oe and  $\sim 0.069$  uem/g at 10 Oe. Thus, the overall diamagnetic signal reveals a superconducting volume fraction of at least  $\sim 60\%$  that has to be attributed to bulk superconductivity.

The emergence of superconductivity explains the drop observed in the resistivity of our powder samples below the superconducting  $T_c$ . This drop is in fact shifted to lower temperatures with increasing the current as can be seen in Fig. 6 (a). The smallness of this drop can be understood as due to the incomplete percolation of the current through our powder samples. In any case, this superconducting feature allows us to trace the onset of superconductivity as a function of pressure from electrical resistivity measurements. Thus, we find that the onset  $T_c$  decreases with pressure in a rather smooth fashion as can be seen in Fig. 6 (b). This behavior has a resemblance to the observed for the orthorhombic distortion [see Fig. 3], and hence suggests a strong interplay be-

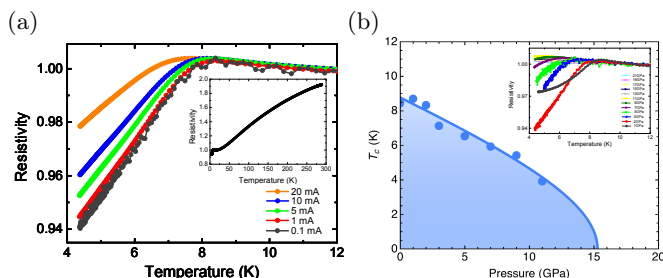


FIG. 6. (a) Low-temperature resistivity for different values of the current applied during the measurements. The inset shows the overall resistivity up to 300 K. Data is normalized to its value at 11 K. (b) Onset temperature of the superconducting transition  $T_c$  as a function of pressure. The onset  $T_c$  is obtained from the intersection of two extrapolated lines reproducing the resistivity in the normal state and the steepest part of the resistivity in the superconducting state.

tween the corresponding instabilities. The re-emergence observed in the orthorhombic distortion, however, is not observed for the superconductivity below 21 GPa.

*Conclusions.*— The synthesis of the novel hydride LaFeSiH inaugurates a supplementary track to understanding the rich physics of iron-based materials. This system displays structural, magnetic and electronic features characteristic of previously reported compounds. Namely, a low-temperature tetragonal to orthorhombic distortion likely related to antiferromagnetic order and a multiband quasi-2D Fermi surface largely dominated by Fe-3d orbitals. Most importantly, this compound demonstrates the possibility of iron-based superconductivity in a pnictogen- and chalcogen-free fashion. Thus, beyond its fundamental significance from both chemistry and physics point of view, LaFeSiH is expected to stimulate further research towards practical applications of iron-based superconducting materials.

We acknowledge ESRF for provision of beamtime at ID27 and M. Mezouar for fruitful discussions. F. B. acknowledges partial support from PRIN Grant No. 2012X3YFZ2\_004 and from the FP7 European project SUPER-IRON (grant agreement No. 283204). A.C. acknowledges support from French Government “Investments for the Future” Program, University of Bordeaux Initiative of Excellence (IDEX Bordeaux), and Sardinia Regional Government “Visiting Professor” Program 2015, University of Cagliari.

\* [andres.cano@cnrs.fr](mailto:andres.cano@cnrs.fr)

- [1] A. Martinelli, F. Bernardini, and S. Massidda, *Comptes Rendus Physique* **17**, 5 (2016); E. Bascones, B. Valenzuela, and M. J. Calderón, *Comptes Rendus Physique* **17**, 36 (2016); D. S. Inosov, *Comptes Rendus Physique* **17**, 60 (2016); A. E. Böhmer and C. Meingast, *Comptes Rendus Physique* **17**, 90 (2016); Y. Gallais and I. Paul, *Comptes Rendus Physique* **17**, 113 (2016); A. van

- Roekeghem, P. Richard, H. Ding, and S. Biermann, *Comptes Rendus Physique* **17**, 140 (2016); F. Rullier-Albenque, *Comptes Rendus Physique* **17**, 164 (2016); S. Zapf, D. Neubauer, K. W. Post, A. Kadau, J. Merz, C. Clauss, A. Löhle, H. S. Jeevan, P. Gegenwart, D. N. Basov, and M. Dressel, *Comptes Rendus Physique* **17**, 188 (2016); P. J. Hirschfeld, *Comptes Rendus Physique* **17**, 197 (2016).
- [2] G. Garbarino, P. Toulemonde, M. Álvarez-Murga, A. Sow, M. Mezouar, and M. Núñez-Regueiro, *Phys. Rev. B* **78**, 100507 (2008); G. Garbarino, R. Weht, A. Sow, A. Sulpice, P. Toulemonde, M. Álvarez-Murga, P. Strobel, P. Bouvier, M. Mezouar, and M. Núñez-Regueiro, *Phys. Rev. B* **84**, 024510 (2011).
- [3] R. Welter, B. Malaman, and G. Venturini, *Solid State Communications* **108**, 933 (1998).
- [4] X. Liu, S. Matsuishi, S. Fujitsu, and H. Hosono, *Phys. Rev. B* **85**, 104403 (2012).
- [5] H. O. Jeschke, I. I. Mazin, and R. Valentí, *Phys. Rev. B* **87**, 241105 (2013).
- [6] S. Iimura, S. Matsuishi, H. Sato, T. Hanna, Y. Muraba, S. W. Kim, J. E. Kim, M. Takata, and H. Hosono, *Nat. Commun.* **3**, 943 (2012).
- [7] M. Hiraishi, S. Iimura, K. M. Kojima, J. Yamaura, H. Hiraka, K. Ikeda, P. Miao, Y. Ishikawa, S. Torii, M. Miyazaki, I. Yamauchi, A. Koda, K. Ishii, M. Yoshida, J. Mizuki, R. Kadono, R. Kumai, T. Kamiyama, T. Otomo, Y. Murakami, S. Matsuishi, and H. Hosono, *Nature Physics* **10**, 300 (2014).
- [8] R. Welter, I. Ijjaali, G. Venturini, and B. Malaman, *Journal of Alloys and Compounds* **265**, 196 (1998).
- [9] S. Tencé, G. André, E. Gaudin, P. Bonville, A. F. Al Alam, S. F. Matar, W. Hermes, R. Pottgen, and B. Chevalier, *Journal of Applied Physics* **106**, 033910 (2009); B. Chevalier, S. Tencé, E. Gaudin, S. Matar, and J.-L. Bobet, *Journal of Alloys and Compounds* **480**, 43 (2009); S. Tencé, S. F. Matar, G. André, E. Gaudin, and B. Chevalier, *Inorganic Chemistry* **49**, 4836 (2010).
- [10] T. Yildirim, *Phys. Rev. Lett.* **101**, 057010 (2008).
- [11] A. Cano, M. Civelli, I. Eremin, and I. Paul, *Phys. Rev. B* **82**, 020408 (2010).